Heliyon 6 (2020) e03294

Contents lists available at ScienceDirect

Heliyon

www.elsevier.com/locate/heliyon

Research article

# First and second-order models for the vortex length in cylinder-on-cone cyclones based on large-eddy simulations

Ellinor Arguilla Svensen, Alex C. Hoffmann *

*Department of Physics and Technology, University of Bergen, Allegaten 55 5007 Bergen, Norway*

ARTICLE INFO

*Keywords:*
Chemical engineering
Mechanical engineering
Mechanics
Applied computing
Computer-aided engineering
Cyclone separators
Natural vortex length
Large-eddy simulations
Multidimensional regression
Model

ABSTRACT

The common design of cyclone separators is the cylinder–on–cone design, and the conical shape has a strong effect on the behavior of the vortex core low in the cyclone. The "vortex length" is the distance between the lip of the gas outlet tube and the position at which the core of the vortex attaches to the wall of the cyclone separation space. This occurs spontaneously at an axial position that, at present, cannot be predicted, although it has a profound effect on the cyclone operation, since, if the vortex is too short, it can lead to plugging and wear. In this paper numerical CFD simulations, using advanced turbulence modeling (LES), are the basis for the formulation of models for the vortex length taking into account the geometrical and operational variables influencing it. The work leads to useful models for the vortex length and reveals important information about which variables determine it and the nature of their effects.

## 1. Introduction

A key aspect for cyclone designers and vendors is to control the vortex end in the cyclone making sure that the vortex penetrates to the bottom of the cyclone separation space giving the optimal separation efficiency and avoiding problems with wear of the wall or plugging in the bottom of the cyclone. This paper will extend the knowledge in this area and investigate the effects of the design and operational variables on the behavior of the vortex in this respect. Earlier work has demonstrated that using an advanced turbulence model, namely LES, CFD can reflect the behavior of the vortex in this respect correctly, even quantitatively, and it was therefore decided to use this technique to simulate the vortex behavior in cylinder–on–cone cyclones for cases where the vortex ended in the separation space itself to elucidate the phenomenon of the "end of the vortex" and the effects of the design and operational variables on it. Fig. 1 shows the geometry of a cylinder-on-cone cyclone and the geometrical notation used in this paper.

Alexander [1] pioneered research on the vortex length in cyclones. He based his work on experiments on fairly small, cylindrical cyclones with diameters in the range 30–50 mm in diameter, limiting the range of applicability of his relation for the vortex length. His paper includes important, more general, research into the flow in cyclones, used as a basis for many studies after him. Among other things, he determined that a smaller vortex finder diameter gives rise to a higher separation efficiency. Alexander defined the natural vortex length, $L_n$ [m], as the distance from the bottom of the vortex finder to the point where the vortex turns, a definition that has been used in most studies since. He also stated that measurements of the vortex turning point were complicated due to the fact that the vortex end moves up and down over range of approximately one quarter of the cyclone diameter. He observed that a large inlet and small outlet give rise to a shortening of the natural vortex length. The relation of Alexander is:

$$\frac{L_n}{D} = 2.23 \left(\frac{D_x}{D}\right) \left(\frac{D^2}{ab}\right)^{\frac{1}{3}} \tag{1}$$

Bryant et al. [2] determined the length of the vortex visually. They fitted an empirical expression to their experimental results. One of their observations was that the position of the end of the vortex is independent of the inlet velocity under normal operation conditions. They compared the theoretical length (as calculated from Alexanders equation) with the length measured by visual inspection of erosion in the conical section and particle deposits on the wall. It was observed that a reduction of the vortex finder diameter gave rise to a longer natural length (contrary to what was observed by Alexander). The cyclones that

* Corresponding author.
*E-mail addresses:* alex. hoffmann@uib.no, alex.hoffmann@ift.uib.no (A.C. Hoffmann).

https://doi.org/10.1016/j.heliyon.2020.e03294
Received 11 August 2019; Received in revised form 17 January 2020; Accepted 21 January 2020

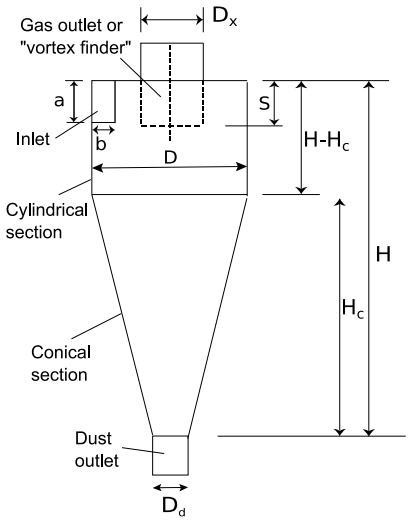


**Fig. 1.** Figure showing the geometrical nomenclature used in this paper, the SI units of all the dimensions are [m], the Reynolds number is defined as $\mathrm{Re} \equiv \frac{\rho v_{in} D_{eq}}{\mu}$ with $v_{in}$ the inlet velocity and $D_{eq}$ the hydraulic equivalent diameter of the inlet, in the geometry used in this paper equal to $4b = 2a$, $\mu$ [kg/ms] is the viscosity and $\rho$ [kg/m$^3$] is the density of the fluid.

were used had a long cylindrical section, and were closer to a swirl tube than a normal cylinder-on-cone design. The relation of Bryant et al. is given in a different form, but can be rewritten to:

$$\frac{L_n}{D} = 2.26 \left(\frac{D_x}{D}\right)^{-1} \left(\frac{D^2}{ab}\right)^{-0.5} \tag{2}$$

Zhongli et al. [3] carried out experiments on long plexiglass cyclones. They proposed an equation suggesting that the natural vortex length was longer than predicted by the equation of Alexander. Experiments were carried out with both cylindrical and conical cyclone designs. The tangential velocity and static pressure were measured with a five-hole pitot probe, and the tangential velocity was seen to decline with axial depth in the cyclone. By charging dust to the cyclone, the vortex was made visible, and a stable dust ring was seen indicating the natural turning point. It was found that the natural length was slightly increased with an increase in the inlet velocity. Larger inlet areas also increased the vortex length. They also observed that a conical cyclone had a longer natural length than a cylindrical one with otherwise the same dimensions. An experimental separation performance study was also conducted with a very low particle concentration [4]. In their study they found that the collection efficiency increased with particle concentration, and the effect of the inlet velocity on the efficiency became less pronounced. The relation given by Zhongli et al. is:

$$\frac{L_n}{D} = 2.4 \left(\frac{D_x}{D}\right)^{-2.25} \left(\frac{D^2}{ab}\right)^{-0.361} \tag{3}$$

Equations (2) and (3) both involve the same dimensionless variables as Alexander's Equation (1), but the effects of both of the variables on the dimensionless vortex length are opposite to those found by Alexander.

Hoffmann et al. [5] performed experiments using glass cyclones visualizing the vortex using smoke. They used a geometry called the Stairmand HE, with a diameter of 0.2 m. Different vortex finder diameters and different lengths of the vortex finder were tested to see the influence on the vortex length. A tube section was placed underneath the conical section to turn the vortex, preventing the vortex core from reaching the surface of the collected dust, reentraining it in the vortex. A stable vortex turning position was often found in the tube section. Smoke was injected to visualize the flow pattern. This was observed to disturb the flow initially, but the position to where the smoke extended was seen fairly clearly after a steady-state flow pattern was reestablished, the smoke remaining in the section under the vortex turning position giving the interesting information that there is very little exchange of gas between the sections above and below the turning position. The smoke left a liquid paraffin layer, on which the flow pattern at the wall could be seen as an alternative visualization method. A circumferential ring formed at a stable position indicating the length of the vortex. However, the ring seemed to appear a few centimeters above the top of the persisting smoke in the bottom section below the vortex end. It was observed that the ring moved lower as the liquid on the wall dried, which was attributed to the apparent roughness, that arose because of the liquid layer, diminishing. In this way it was found that the vortex end was dependent on wall roughness. The natural length was found to be longer with larger vortex finder diameter and inlet velocities. Alexanders equation predicted a shorter vortex than was found experimentally. Using dust for visualization instead of smoke, the same phenomena were observed. An amount of dust was deposited on the wall from the dust collection vessel up to at certain position in the tube section under the cyclone dust exit. With a high dust loading, the position of the vortex end was further up in the cyclone than without dust present, confirming that the higher apparent wall roughness due to the dust on the wall gives rise to a shorter vortex.

Peng et al. [6, 7] used a stroboscope to visualize the vortex core in cylinder–on–cone cyclones and swirl tubes, and pressure transducers to measure the pressure on the wall. When using the stroboscope a small ring in the plane of the wall could be seen in dust on the wall, which was the core of the vortex ("eye of the hurricane"), its fast precessing motion, normally making it invisible to the naked eye, was frozen by the strobe-light when the frequency was set exactly right. They used pressure transducers to detect the rotation frequency of the precessing vortex core. In the middle of the core there is low pressure and the rotation could be measured as a sudden drop in wall pressure each time the vortex core passed the angular position of the pressure tapping. By using multiple transducers placed vertically along the cyclone body an axial profile for the wall pressure was obtained from which the axial position of the vortex turning point (vortex "end") could be found.

Qian et al. [8] used response surface design to analyze the results from their CFD simulations to obtain a new model for the vortex length. A Reynolds stress transport (RSM) turbulence model was used. The variables chosen were: the vortex finder diameter ($D_x$), the inlet length and width ($a$ and $b$), the vertical length of the cylindrical section of the cyclone body beneath the vortex finder ($H - H_c - S$) and the Reynolds number (Re). They found that the natural length varies slightly with the inlet velocity, and that with increasing vortex finder diameter the length increased to a certain point and after this it becomes shorter. For the inlet area the findings were consistent with the relation of Alexander, smaller inlet areas results in an increase of the vortex length. In all the simulations the vortex ended in the tube section attached to the dust exit under the cyclone body like the design used by Peng et al.

An experimental study focusing on the effects of the inlet section angle on the separation performance was also performed [9]. In most cyclone designs the inlet section is perpendicular to the cyclone axis but in this study other angles, whereby the inlet was pointing slightly downwards towards the dust outlet, were tested. They found that the tangential velocity decreased in some regions with increasing angle. The tangential velocity in the outer vortex increased and that in the inner vortex decreased. They also found that the pressure drop was reduced compared to a normal cyclone, and this difference increased with larger angles. The separation efficiency also increased significantly with increasing inlet angle. Using CFD and a response surface methodology the inlet section angle could be studied more comprehensively [10], they found that a conventional cyclone had a stronger short-cut flow rate (see [11]) than cyclones with angled inlets. The vortex length was not studied in this work. Also Bernado et al. [12] studied the effect of the inlet angle on the working of cyclones using CFD.

Earlier work in the group of the present authors [13, 14] has shown that, while both LES and RSM turbulence models can simulate the end

of the vortex phenomenon correctly, LES gives results which are quantitatively better in line with experiment than RSM, which is not surprising in light of the fact that LES, while being much more demanding in terms of computer power, is more consistent with the physics of the flow field, requiring only a simple turbulence model for the effects of the subgrid-scale turbulence, which is almost isotropic. This is supported in the comprehensive comparison of CFD methods for cyclone flow simulation by Gronald and Derksen [15]. Since experiments had shown that the wall roughness has a strong effect on the vortex length, CFD simulations were also performed to cast light on this effect. Simulations with walls having absolute roughnesses of 0.1 and 0.2 mm were carried out for varying inlet velocities [13, 16], the simulation results confirming the experimental result that increasing the wall roughness shortens the natural length of the vortex.

Response surface methods represent a robust and highly empirical method for identifying the salient variables governing almost any process parameter of interest and constructing predictive models [17, 18, 19]. These methods have become very popular in the research literature recently.

Chandrasekharan et al. [20] used response surface methods to study and optimize the performance of coal fired thermal power plants as functions of the operating variables. They combined their overall model with models for the individual processing units for design purposes.

Sonsiri et al. [21] studied aspects of the working of a rotary dryer, such as the moisture content of the product and the electrical power used, as functions of the operation of associated process equipment, namely a cyclone blower and a biogas blower.

Such studies illustrate the power and the broad range of applicability of the response surface method, and explain the growing popularity of the methodology.

Some of the most relevant works wherein CFD simulations are used to study instabilities in confined flows and the flow in cyclone separators will now be discussed briefly emphasizing the reliability of LES simulations [22].

Griffiths et al. [23] performed a study using CFD to study cyclone performance in small sampling cyclones. They mention, as is also well known [24], that the standard k-$\epsilon$ turbulence model causes excessive levels of turbulent viscosity and an unrealistic tangential velocity distribution and can therefore not be used. Since Reynolds Stress models at the time were very computationally expensive, an RNG-based k-$\epsilon$-model was used.

Hoekstra et al. performed an experimental study which verified CFD simulations [25]. They used cyclones of 0.29 m in diameter with a scroll type of inlet (see [11]). The cyclones had a long cylindrical section with a short conical section. Experiments were carried out at a Reynolds number of $2.5\times10^4$. Tangential and axial velocity components along the radial direction were measured using laser-Doppler anemometry (LDA). CFD simulations were also carried out using different turbulence models, namely the k-$\epsilon$-model, the RNG-k-$\epsilon$-model and the Reynolds Stress Transport Model (RSM). Comparing the experiments with the CFD simulations carried out with RSM, they found good agreement. The other turbulence models did not reflect the axial and tangential velocities accurately and were therefore not found suitable.

In his PhD thesis [26] Hoekstra performed an extensive study on cyclone efficiency, both experimentally and by CFD. The gas flow field was studied experimentally using LDA and he found a low-frequency instability, related to a phenomenon called the precessing vortex core (PVC). This PVC-phenomenon was further studied using LDA.

CFD simulations were performed using different turbulence models to compare with the experimental data, good agreement was found when using the Reynolds Stress transport turbulence model. The LES-model was also found to be able to model the precessing motion of the vortex core. From this a regression model was formulated to describe the collection efficiency of the cyclone. A response surface model (to test the effects of different geometric variables and operating conditions) was also presented, which could predict the pressure drop and the cut-size of the Stairmand cyclone.

Derksen et al. [27] used LES to simulate turbulent flow in a reverse-flow cyclone. The cyclone was of the swirl tube type, but with a tangential (scroll-type) inlet instead of swirl vanes (see [11]). The Reynolds number of the flow was $1.4\times10^4$. A three-dimensional simulation with high resolution was used, and it was found that an axi-symmetrical model would not properly model the swirling flow. Good agreement with the LDA-experiments executed by Hoekstra [25] was found. The study also included simulations with particles in the flow, and it was found that particles larger 10 μm did not need any special modeling. However, smaller particles would influence the subgrid-scale turbulence of the LES simulations and this had to be taken in to account. It was mentioned that flows at higher (and more common in industrial cyclones) Reynolds numbers, was not straight-forward to simulate using a uniformly spaced grid because of the lack of resolution in the boundary layer. Locally refined grid was recommended as a solution. A more extensive study with simulations using LES was subsequently done [28]. It is mentioned in this work that using LES for swirling flow is better than using RMS because flow containing particles is more realistically modeled with LES, also swirling flows often experience coherent, quasi-periodic fluctuations (such as the precessing of the vortex core, PVC) which LES simulates better than RMS. Three different subgrid-scale (SGS) turbulence models where used, using the same damping function. They also observed the phenomenon of vortex breakdown in the simulations. When the effect of the diameter of the vortex finder diameter was tested, they found that the axial velocity was strongly dependent on this and also on the axial position of the vortex tube. The Mixed-scale-model (MSM) was the best of the SGS-models tested. They also found that LES revealed more of the physics in turbulent flow than other models, but at a computational cost [15, 29].

This present work aims to make use of the advancing computer power to formulate an improved model for the natural vortex length in cylinder-on-cone cyclones based on CFD simulations using state-of-the-art turbulence modeling, namely LES. A response surface method similar to that in ref. [8] will be used to formulate both first-order and second-order models for the vortex length and to advance physical insight into the factors affecting the vortex length and the nature of their effects. In addition, models of different functional forms fitted to the numerical results will be explored with the goal of finding an optimal model for use in practice.

## 2. Numerical methods

The equations to be solved numerically are the Navier-Stokes equations:

$$\begin{aligned}&\nabla\cdot\mathbf{v}=0\\&\rho\frac{D\mathbf{v}}{Dt}=\rho\mathbf{g}-\nabla p+\mu\nabla^2\mathbf{v}\end{aligned}\tag{4}$$

A numerical mesh is applied to cover the domain of interest, and discrete representations of the equations are solved on the mesh. The mesh has to be fine enough to obtain an accurate solution, and as coarse as possible to limit the computational effort.

### 2.1. Meshing, time discretization and boundary treatment

The commercial CFD package Star-CCM+ was used for the numerical simulations. This package offers mesh cells of a variety of shapes, for example hexahedra, tetrahedra or blocks. Which of these types is optimal depends on the geometry of the domain. Also unstructured grids are offered. The meshing models used in this work are “surface remesher”, “trimmer” and “prism layer mesher”. The trimmer offers the option of using a regular grid, which is advantageous, at the same time as ensuring that the cells do not extend beyond the computational domain. The prism layer mesher makes it possible to have smaller, prism shaped,

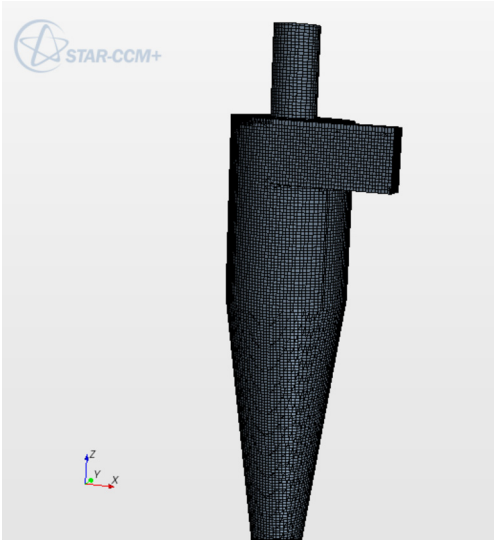


**Fig. 2.** Figure showing the mesh on the boundary of the computational domain.

cells near the wall. A prism layer is orthogonal prismatic cells close to the wall, for which a different size than the core cells can be set. The surface mesh is shown in Fig. 2.

The method for wall treatment in the LES turbulence model is described in more detail elsewhere [13]. Briefly, the shear velocity, $u_\tau$, is estimated from inverting a third-order Spalding wall function:

$$y^+ = u^+ + \frac{1}{E}\left(\exp(ku^+) - 1 - ku^+ - \frac{(ku^+)^2}{2!} - \frac{(ku^+)^3}{3!}\right) \quad (5)$$

where $E$ is an empirical factor and $k$ is the von Karman constant. The momentum flux from the wall is then calculated from the estimated $u_\tau$. Comparison with experiment demonstrated that it is important that the wall velocity is evaluated at the appropriate $y^+$ value when determining the velocity gradient at the wall.

Grid dependency tests were carried out, and it was found that the largest cell size giving grid-independent results for the end-of-vortex phenomenon was 4.5 mm cells, corresponding to a total of 500000 cells. An implicit scheme was used, and the time-step set so that the Courant-number did not exceed 1.5.

### 2.2. Turbulence modeling

As mentioned above, earlier simulations and experiments [13] have shown that, although unsteady simulations using Reynolds stress turbulence modeling (RSM) can correctly reflect the end-of-vortex (EoV) phenomenon, namely the vortex core bending spontaneously to the cyclone wall and precessing around the wall at a more or less fixed axial position, quantitative agreement between simulation and experiment for the position of the EoV is better when using Large-eddy simulations (LES).

For large eddy simulations of the flow of incompressible fluids a spatial filter is applied to the flow variables. For an arbitrary flow variable, $\phi(\mathbf{x})$, which could be a component of the fluid velocity or the pressure, the spatial filter is:

$$\bar{\phi} = \int G(\mathbf{x} - \mathbf{x}', \Delta)\phi(\mathbf{x}, t)d\mathbf{x}' \quad (6)$$

where $G(\mathbf{x})$ is some suitable function of the spatial coordinates, related to the size of one computational cell. $\Delta$ is the width of the filter, similar in magnitude to the size of the computational cells. By applying this filter turbulent eddies smaller than the grid size are filtered out, and their effect on the flow is modeled with a turbulence model. This model, however, can be quite simple, since this fine-scale turbulence is almost isotropic. In this work the well-known and very simple Smagorinsky subgrid turbulence model was used. The larger eddies are in LES simulated directly.

**Table 1**
List of the simulations carried out during this work and the results for the dimensionless vortex length.

| No. | $D_x/D$ | $(H-H_c)/D$ | $H_c/D$ | $(ab)^{0.5}/D$ | Re | $L_n/D$ |
|---|---|---|---|---|---|---|
| 1 | 0.3 | 1.0 | 2.0 | 0.2 | 30000 | 2.5 |
| 2 | 0.5 | 1.0 | 2.0 | 0.2 | 30000 | 2.5 |
| 3 | 0.3 | 3.0 | 2.0 | 0.2 | 30000 | 4.5 |
| 4 | 0.5 | 3.0 | 2.0 | 0.2 | 30000 | 4.5 |
| 5 | 0.3 | 1.0 | 5.0 | 0.2 | 30000 | 2.02 |
| 6 | 0.5 | 1.0 | 5.0 | 0.2 | 30000 | 2.48 |
| 7 | 0.3 | 3.0 | 5.0 | 0.2 | 30000 | 4.17 |
| 8 | 0.5 | 3.0 | 5.0 | 0.2 | 30000 | 4.53 |
| 9 | 0.3 | 1.0 | 2.0 | 0.55 | 30000 | 1.17 |
| 10 | 0.5 | 1.0 | 2.0 | 0.55 | 30000 | 1.32 |
| 11 | 0.3 | 3.0 | 2.0 | 0.55 | 30000 | 1.62 |
| 12 | 0.5 | 3.0 | 2.0 | 0.55 | 30000 | 1.58 |
| 13 | 0.3 | 1.0 | 5.0 | 0.55 | 30000 | 1.47 |
| 14 | 0.5 | 1.0 | 5.0 | 0.55 | 30000 | 1.28 |
| 15 | 0.3 | 3.0 | 5.0 | 0.55 | 30000 | 1.88 |
| 16 | 0.5 | 3.0 | 5.0 | 0.55 | 30000 | 1.75 |
| 17 | 0.3 | 1.0 | 2.0 | 0.2 | 3000000 | 2.50 |
| 18 | 0.5 | 1.0 | 2.0 | 0.2 | 3000000 | 2.50 |
| 19 | 0.3 | 3.0 | 2.0 | 0.2 | 3000000 | 4.50 |
| 20 | 0.5 | 3.0 | 2.0 | 0.2 | 3000000 | 2.50 |
| 21 | 0.3 | 1.0 | 5.0 | 0.2 | 3000000 | 2.06 |
| 22 | 0.5 | 1.0 | 5.0 | 0.2 | 3000000 | 2.86 |
| 23 | 0.3 | 3.0 | 5.0 | 0.2 | 3000000 | 3.05 |
| 24 | 0.5 | 3.0 | 5.0 | 0.2 | 3000000 | 3.45 |
| 25 | 0.3 | 1.0 | 2.0 | 0.55 | 3000000 | 2.50 |
| 26 | 0.5 | 1.0 | 2.0 | 0.55 | 3000000 | 2.50 |
| 27 | 0.3 | 3.0 | 2.0 | 0.55 | 3000000 | 2.08 |
| 28 | 0.5 | 3.0 | 2.0 | 0.55 | 3000000 | 1.92 |
| 29 | 0.3 | 1.0 | 5.0 | 0.55 | 3000000 | 3.10 |
| 30 | 0.5 | 1.0 | 5.0 | 0.55 | 3000000 | 2.11 |
| 31 | 0.3 | 3.0 | 5.0 | 0.55 | 3000000 | 2.18 |
| 32 | 0.5 | 3.0 | 5.0 | 0.55 | 3000000 | 1.68 |
| 33 | 0.4 | 2.0 | 3.5 | 0.35 | 1515000 | 2.11 |
| 34 | 0.3 | 2.0 | 3.5 | 0.35 | 1515000 | 2.88 |
| 35 | 0.5 | 2.0 | 3.5 | 0.35 | 1515000 | 2.00 |
| 36 | 0.4 | 1.0 | 3.5 | 0.35 | 1515000 | 3.05 |
| 37 | 0.4 | 3.0 | 3.5 | 0.35 | 1515000 | 2.26 |
| 38 | 0.4 | 2.0 | 2.0 | 0.35 | 1515000 | 3.00 |
| 39 | 0.4 | 2.0 | 5.0 | 0.35 | 1515000 | 2.11 |
| 40 | 0.4 | 2.0 | 3.5 | 0.2 | 1515000 | 5.00 |
| 41 | 0.4 | 2.0 | 3.5 | 0.55 | 1515000 | 3.28 |
| 42 | 0.4 | 2.0 | 3.5 | 0.35 | 30000 | 1.85 |
| 43 | 0.4 | 2.0 | 3.5 | 0.35 | 3000000 | 5.00 |

## 3. Simulations

A total of 43 simulations were carried out to conform with a "central composite" experimental design, which was seen as the simplest design to give useful information about the effects of all the salient variables and is a scheme similar to that used in [8]. The geometrical and operational variables were chosen so as to cover the range of geometries used in practice as given in [11]. The simulations and the results are listed in Table 1. The nomenclature is, as mentioned, given in Fig. 1. If the vortex end is not seen in the cyclone the vortex is said to be "centralized", although in our experience it is then normally attached to the dust outlet lip, except in cases where the dust collection vessel is very shallow allowing the vortex to penetrate it and end on the bottom of the dust hopper or on the surface of the collected dust in it (which is not good).

## 4. Results

An example simulation is shown in Fig. 3, the vortex core is clearly visible in this contour plot for the static pressure and is seen to bend from the axis of the cyclone and attach to the conical part of the wall.

The results of the simulations are listed in Table 1.

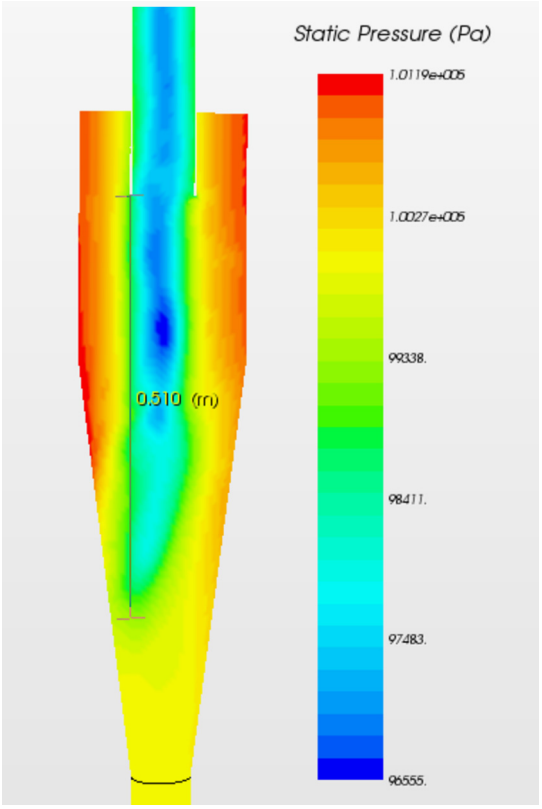


**Fig. 3.** Example simulation snapshot, the low-pressure vortex core is clearly visible and is seen to bend from the cyclone axis and attach to the conical part of the wall. The length of the vortex, from the lip of the vortex finder to the point of attachment is indicated. The simulation is for an inlet velocity, $v_{in}$, of 20 m/s.

During the simulations the following observations were made:

- In the simulations with low Re the vortex took some time to form inside the cyclone body.
- For the simulations with high Re the vortex formed almost immediately both when the vortex core was centralized and when it attached to the wall to form the EoV.
- All the shorter cyclones experienced a centralized vortex, in the most of the longer cyclones the EoV phenomenon was seen.
- A longer conical section seemed to destabilize the vortex and gave rise to a shorter natural vortex length.

## 5. Discussion and formulation of models

In this section a series of model equations will be fitted to the numerical results for the vortex length, attempts will be made to find relatively simple model equations that nevertheless are useful in practice. The method will be to fit the models to the simulation results using the robust zeroth-order multidimensional search technique devised by Rosenbrock [30], for this the natural logarithm was taken of the Reynolds number to avoid round-off-errors arising from order-of-magnitude discrepancies in the independent variables. An analysis-of-variance table generated for the second order model by the software SPSS will also be used.

### 5.1. First-order model

The first model to be fitted will be a first-order model, the model is constructed as a series of additive first-order terms where all the adjustable parameters have been fitted to best match the simulation results for the length of the vortex, $L_n$:

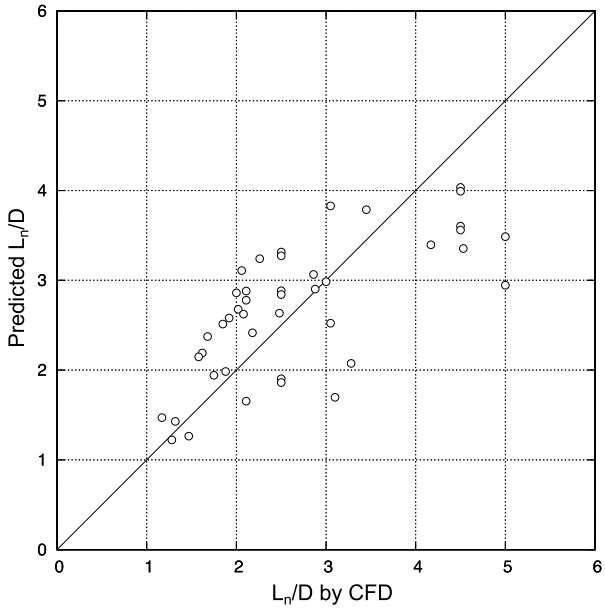


**Fig. 4.** Parity plot for the fitted first order model, Equation (8).

$$\frac{L_n}{D} = p_1 + \sum_{i=1}^{5} p_{i+1} \times x_i \tag{7}$$

where the $p_i$ are the adjustable parameters and the $x_i$ are the independent geometrical and operational variables listed in Table 1.

The fitted first-order model is:

$$\frac{L_n}{D} = 2.56 - 0.212\left(\frac{D_x}{D}\right) - 0.360\left(\frac{H - H_c}{D}\right) - 0.0688\left(\frac{H_c}{D}\right) - 4.03\left(\frac{(ab)^{0.5}}{D}\right) + 0.0938\,(\ln \mathrm{Re}) \tag{8}$$

The Pearson's r is 0.701, the residual sum of squares is 24.46 and a parity plot is shown in Fig. 4. The fit is seen to be reasonable without having a very high predictive power for use in practice.

The qualitative effects, however, on the natural vortex length of the variables can be gleaned from this relationship, an increase in $D_x$ appears to weakly decrease the length of the vortex, while an increase in the cylindrical-section height, $(H - H_c)$ does the same. An increase in the dimensionless inlet area has a stronger effect in decreasing the natural vortex length, while an increase in Re increases the natural length. The effects of $D_x$ and $ab$ are qualitatively consistent with the relation of Zhongli et al. and Bryant et al., but not with that of Alexander although it does agree with the text of Alexanders' paper as quoted in the Introduction, while that of Re is consistent with literature in general.

It can be concluded from this that the variables chosen in this study do influence the length of the vortex, and the first-order model does reflect their effects, but that this model is not sufficient to reduce the residual variance in the results to a low value. Also the famous model of Alexander does not seem to apply to cylinder-on-cone cyclones (see also below).

### 5.2. Second-order model

The first-order model does not reduce the residual variance so much that it gives a sufficiently good description of the length of the vortex, and this can be the motivation to explore a second-order model where also the non-linear effects of the variables and their interactions are taken into account. The draw-back of constructing such a model is that it is very complex and involves a large number of adjustable parameters.

The form of this model, which is similar to the one investigated by Qian et al. [8] is:

$$\frac{L_n}{D} = p_1 + \sum_{i=1}^{5}\sum_{j=i}^{5} p_{ij} \times x_i x_j \tag{9}$$

This, in principle, involves 21 adjustable parameters, a very large number. For the multidimensional search the choice is made here to reduce this a little by deciding in advance, based on preliminary fit results, that the two-factor interactions: $(D_x/D)((H-H_c)/D)$ and $(D_x/D)(H_c/D)$ are not important, reducing the number of parameters to 19.

Two methods were used to fit this second-order model to the simulation results: a multi-dimensional search as for the other models and using the commercial software SPSS. The multidimensional search required in excess of 2 million iterations, but is coded in a compiled language, namely FORTRAN, which executes faster than any other language except C/C++, which executes at about the same speed. The result of the search was:

$$\begin{aligned}\frac{L_n}{D} = {} & 12.6 + 54.5\left(\frac{D_x}{D}\right) + 4.71\left(\frac{H-H_c}{D}\right) + 1.97\left(\frac{H_c}{D}\right) - \\ & 32.0\left(\frac{\sqrt{ab}}{D}\right) - 3.71\ln(\mathrm{Re}) - 61.8\left(\frac{D_x}{D}\right)^2 - 6.70\left(\frac{D_x}{D}\right)\left(\frac{\sqrt{ab}}{D}\right) - \\ & 0.216\left(\frac{D_x}{D}\right)\ln(\mathrm{Re}) - 0.483\left(\frac{H-H_c}{D}\right)^2 - 0.050\left(\frac{H-H_c}{D}\right)\left(\frac{H_c}{D}\right) - \\ & 2.56\left(\frac{H-H_c}{D}\right)\left(\frac{\sqrt{ab}}{D}\right) - 0.1017\left(\frac{H-H_c}{D}\right)\ln(\mathrm{Re}) - 0.258\left(\frac{H_c}{D}\right)^2 - \\ & 0.502\left(\frac{H_c}{D}\right)\left(\frac{\sqrt{ab}}{D}\right) - 0.0251\left(\frac{H_c}{D}\right)\ln(\mathrm{Re}) + 36.1\left(\frac{\sqrt{ab}}{D}\right)^2 - \\ & 0.542\left(\frac{\sqrt{ab}}{D}\right)\ln(\mathrm{Re}) + 0.158(\ln(\mathrm{Re}))^2\end{aligned} \tag{10}$$

The Pearson's r is 0.911, the residual sum of squares is 8.105 and a parity plot is shown in Fig. 5. The fit is seen to be good.

The second method of fitting Equation (9) to the simulation results was using the commercial software SPSS. The results of this is shown in Table 2, the residual sum of squares is 8.110.

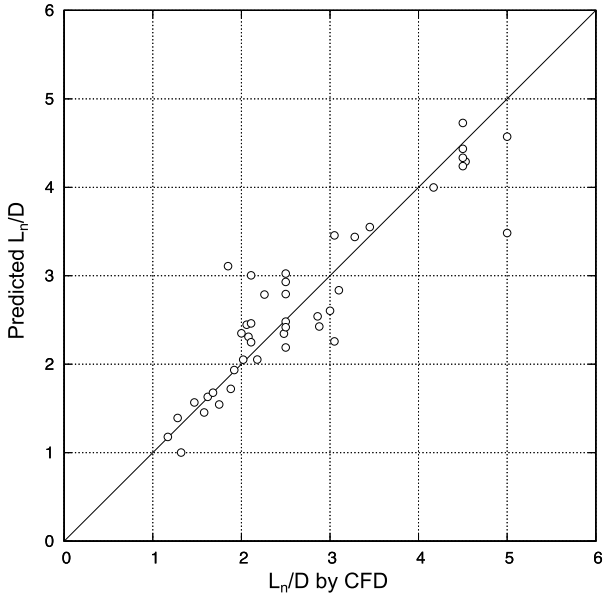


**Fig. 5.** Parity plot for the fitted second order model, Equation (10).

Comparing Equation (10) and the unstandardized coefficients in Table 2 it is clear that the coefficients are similar between the two, the multidimensional search has achieved a slightly lower residual sum of squares than SPSS in spite of two interactions having been disregarded. A direct comparison with the fit of a similar model by Qian et al. [8] is not possible, since the variables chosen in this study are different from theirs. The results in Table 2 make it possible to concentrate on the most significant effects on the vortex length, this will be explored later in this paper.

### 5.3. Equation of Alexander, Bryant et al., and Zhongli et al.

These three models have the same functional form and depend on the same dimensionless independent variables [1, 2, 3]:

$$\frac{L_n}{D} = p_1\left(\frac{D_x}{D}\right)^{p_2}\left(\frac{D^2}{ab}\right)^{p_3} \tag{11}$$

**Table 2**
Results of fitting the second order model to the simulation results using SPSS, the degrees for freedom for the $t$-value is 22.

| Variable | Unstandardized Coefficients | Std. error | Standardized Coefficients | $t$ | Significance Level, p-value |
|---|---|---|---|---|---|
| Constant | 12.05 | 20.37 | | .584 | .565 |
| $(D_x/D)$ | 59.55 | 31.82 | 4.998 | 1.872 | .075 |
| $(D_x/D)^2$ | -68.06 | 38.75 | -4.577 | -1.756 | .093 |
| $((H-H_c)/D)$ | 4.693 | 1.748 | 3.938 | 2.685 | .014 |
| $((H-H_c)/D)^2$ | -.468 | .387 | -1.582 | -1.208 | .240 |
| $(H_c/D)$ | 1.905 | 1.318 | 2.398 | 1.445 | .162 |
| $(H_c/D)^2$ | -.252 | .172 | -2.236 | -1.466 | .157 |
| $(\sqrt{ab}/D)$ | -32.373 | 10.690 | -4.765 | -3.028 | .006 |
| $(\sqrt{ab}/D)^2$ | 36.61 | 12.93 | 4.091 | 2.832 | .010 |
| ln(Re) | -3.747 | 3.638 | -7.59 | -1.030 | .314 |
| $\ln(\mathrm{Re})^2$ | .159 | .144 | 8.090 | 1.104 | .281 |
| $(D_x/D)((H-H_c)/D)$ | -.095 | 1.073 | -.037 | -.089 | .930 |
| $(D_x/D)(H_c/D)$ | .055 | .716 | .033 | .077 | .939 |
| $(D_x/D)(\sqrt{ab}/D)$ | -6.733 | 6.130 | -.459 | -1.098 | .284 |
| $(D_x/D)\ln(\mathrm{Re})$ | -.221 | .460 | -.298 | -.479 | .636 |
| $((H-H_c)/D)(H_c/D)$ | -.049 | .072 | -.201 | -.691 | .496 |
| $((H-H_c)/D)(\sqrt{ab}/D)$ | -2.563 | .613 | -1.161 | -4.182 | .000 |
| $((H-H_c)/D)\ln(\mathrm{Re})$ | -.102 | .046 | -1.176 | -2.211 | .038 |
| $(H_c/D)(\sqrt{ab}/D)$ | .505 | .409 | .368 | 1.236 | .230 |
| $(H_c/D)\ln(\mathrm{Re})$ | -.025 | .031 | -.444 | -.818 | .422 |
| $(\sqrt{ab}/D)\ln(\mathrm{Re})$ | .543 | .263 | 1.104 | 2.066 | .051 |

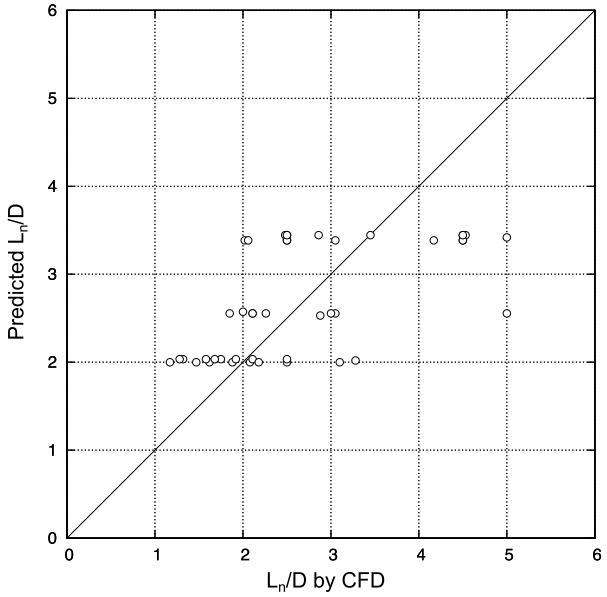


**Fig. 6.** Parity plot for the fitted equation of the form of Alexander/Zhongli et al./Bryant et al., Equation (12).

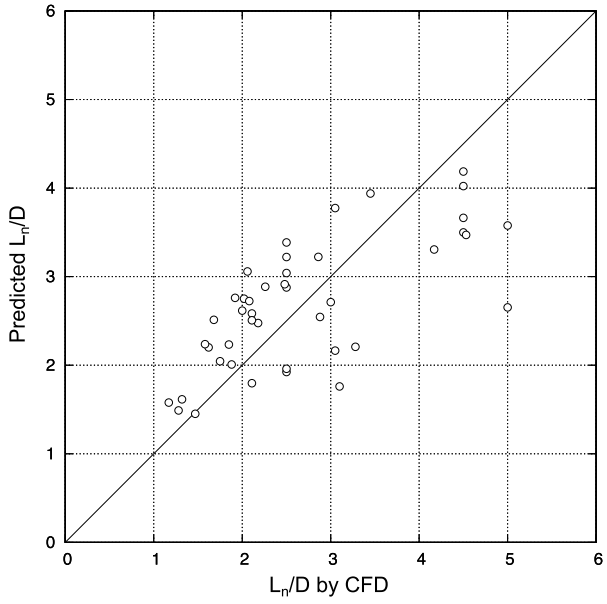


**Fig. 7.** Parity plot for the fitted equation of the form of Equation (13), an equation to improve Alexanders equation to take into account additional parameters in cylinder-on-cone cyclones.

Whether a model of this form can predict the length of the vortex in cylinder-on-cone cyclones can be explored by fitting the parameters to the simulation results. The result of doing this is:

$$\frac{L_n}{D} = 1.53\left(\frac{D_x}{D}\right)^{0.0338}\left(\frac{D^2}{ab}\right)^{0.260} \tag{12}$$

The Pearson's r for this fit is 0.5942, the residual sum of squares is 31.16 and the parity plot is shown in Fig. 6. The parity plot has the clear characteristics of a fit wherein the effects of some of the important governing variables have not been taken into account, and it can be concluded that this functional form is not sufficient to predict the length of the vortex in cylinder-on-cone cyclones. The effects of the physical variables on the RHS agree qualitatively with the relation of Alexander. As mentioned, however, this relation has limited value for the prediction of the natural vortex length in cylinder-on-cone cyclones in practice.

The question could be posed if it is possible to modify this standard expression to take into account the effect of other variables. To explore this further a model equation wherein the effects of other variables are accounted for in an additive product-of-powers term, implicitly assuming that their effects can be superposed on the effects of the two parameters featuring in the standard expression, was formulated and fitted to the simulation results. This equation is of the form:

$$\frac{L_n}{D} = p_1\left(\frac{D_x}{D}\right)^{p_2}\left(\frac{D^2}{ab}\right)^{p_3} + p_4\Pi_{i=3}^{5}x_i^{p_{i+2}} \tag{13}$$

featuring an additive product-of-powers term to take into account the effects of the other variables considered in this study. The result of fitting Equation (13) to the simulation results is:

$$\frac{L_n}{D} = 0.195\left(\frac{D_x}{D}\right)^{0.182}\left(\frac{D^2}{ab}\right)^{0.737} + 0.743\left(\frac{H-H_c}{D}\right)^{0.380}\times \left(\frac{H_c}{D}\right)^{-0.122}((\ln(\mathrm{Re}))^{0.0548} \tag{14}$$

resulting in a fit with a Pearsons r of 0.697, a residual sum of squares of 24.8 and the parity plot shown in Fig. 7.

This is clearly an improvement compared with the original form of the equation of Alexander, Zhongli et al. and Bryant et al., as would be expected.

### 5.4. Other functional forms

The simulation results allow us to try out different functional forms in a quest to find a relatively simple predictive relation for the natural vortex length in cylinder-on-cone cyclones.

#### 5.4.1. Product-of-powers

A simple product-of-powers expression is often used in multi-dimensional regression. The functional form is:

$$\frac{L_n}{D} = p_1\Pi_{i=1}^{5}x_i^{p_{i+1}} \tag{15}$$

with a total of 6 adjustable parameters. This form should offer quite a lot of flexibility at the same time as not involving too many adjustable parameters, in fact only six for the present case. The result of fitting this relation to the simulation results was:

$$\frac{L_n}{D} = 1.28\left(\frac{D_x}{D}\right)^{0.0256}\left(\frac{H-H_c}{D}\right)^{0.309}\left(\frac{H_c}{D}\right)^{-0.0948}\left(\frac{\sqrt{ab}}{D}\right)^{-0.565}\ln(\mathrm{Re})^{0.0225} \tag{16}$$

Pearson's r for this fit is 0.7371, the residual sum of squares is: 22.03, and the parity plot is shown in Fig. 8 A). This fit is better than the other expressions discussed hitherto in this paper, except for the second-order models.

#### 5.4.2. Identifying the most important variables and interactions

Studying the results of the statistical analysis in Table 2 and identifying the most important variables influencing the length of the vortex the following variables and interactions were identified, based on the significance levels of their effects: $(D_x/D)$, $(H-H_c)/D$, $\sqrt{ab}/D$, $(D_x/D)^2$, $((H-H_c)/D)^2$, $(\sqrt{ab}/D)^2$ and $((H-H_c)/D)(\sqrt{ab}/D)$. A model equation involving only these effects and interactions was fitted to the simulation results. The result was:

$$\frac{L_n}{D} = -11.5 + 82.3\left(\frac{D_x}{D}\right) + 1.31\left(\frac{H-H_c}{D}\right) - 16.3\left(\frac{\sqrt{ab}}{D}\right) - 99.9\left(\frac{D_x}{D}\right)^2 + 26.7\left(\frac{\sqrt{ab}}{D}\right)^2 - 6.71\left(\frac{D_x}{D}\right)\left(\frac{\sqrt{ab}}{D}\right) - 2.56\left(\frac{H-H_c}{D}\right)\left(\frac{\sqrt{ab}}{D}\right) \tag{17}$$

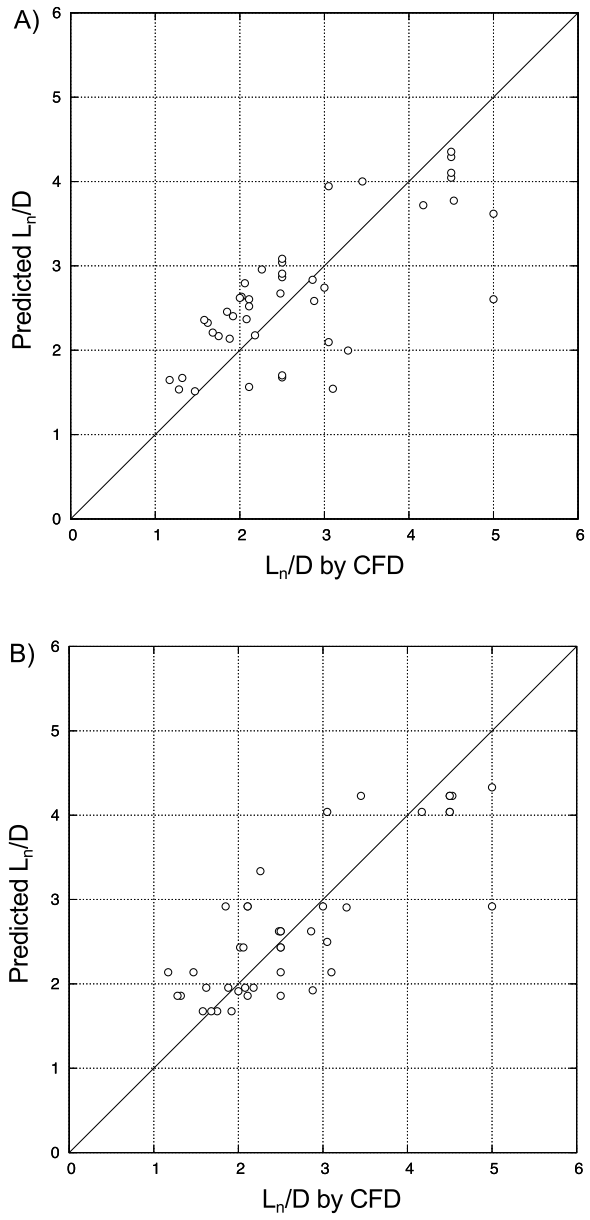


**Fig. 8.** Parity plots for the fitted equations of the forms A): product-of-powers and B): selected parameters and interactions.

The Pearson's r for this fit was 0.814 and the residual sum of squares was 16.3. The parity plot is shown in Fig. 8 B). Although not appearing that good in the figure, this is the closest fit to the simulation results except for that of the second-order models.

## 6. Further discussion

It is a well-established procedure to "spot the result that is not in the family of results" and eliminate this result before the regression analysis is carried out, based on the argument that this eliminates an odd result that might well be wrong for a variety of reasons and therefore should not influence the regression parameters. In the present case this would be the result of the very last simulation in Table 1, which was also chronologically the last simulation to be carried out. If this result was disregarded, the Pearson's r values would be significantly higher, and the residual sum of squares considerably lower than the values quoted in this paper, for example, for the second-order model in Equation (10) Pearson's r would be 0.959 and the residual sum of squares would be 3.46. The choice has been made not to do this in this paper, but it may be kept in mind that the fits would be better if this was done.

## 7. Conclusions

This work has clearly demonstrated that the classical form of models to predict the length of the vortex in cyclones, namely Equation (11), is insufficient for cylinder-on-cone cyclones, the type of cyclone almost universally used these days, and that other variables, both geometrical and operational, need to be taken into account for this type of cyclone.

The second-order model, Equation (10) gave a very good fit and should predict the dimensionless vortex length in cylinder-on-cone cyclones quite well, but it is unwieldy, involving 19 adjustable parameters. None of the simpler functional forms tested in this work gave as good a fit to the simulation results. The best of the simplified models tested has been shown, by the Pearson's r-values given, to be Equation (17), involving only the variables that were found to be the most significant in determining the length of the vortex. This equation, although not as good as the second-order-model in Equation (10), may be used in practice as a guide for the design of cylinder-on-cone cyclones.

## Declarations

### *Author contribution statement*

A. Hoffmann: Conceived and designed the experiments; Analyzed and interpreted the data; Wrote the paper.

E.A. Svensen: Performed the experiments; Analyzed and interpreted the data; Wrote the paper.

### *Funding statement*

This research did not receive any specific grant from funding agencies in the public, commercial, or not-for-profit sectors.

### *Competing interest statement*

The authors declare no conflict of interest.

### *Additional information*

No additional information is available for this paper.

## Acknowledgements

The authors wish to extend their gratitude to Dr Gleb Pisarev and Torill Rødland for help with experimental work in support of the simulations.

## References

[1] R. Mck Alexander, Fundamentals of cyclone design and operation, in: Proceedings Aus. I.M.M., 1949.

[2] H.S. Bryant, R.W. Silverman, F.A. Zenz, How dust in gas affects cyclone pressure drop, Hydrocarbon Process 62 (1983) 87–90.

[3] J. Zhongli, W. Xiaolin, S. Mingxian, Experimental research on the natural turning length in the cyclone, in: Proceedings of Filtech Europa 91, vol. 2, 1991, pp. 583–589.

[4] Z.L. Ji, Z. Xiong, X. Wu, H. Chen, H. Wu, Experimental investigations on a cyclone separator preformance at an extremely low particle consentration, Powder Technol. 191 (2009) 254–259.

[5] A.C. Hoffmann, R. Dejonge, H. Arends, C. Hanrats, Evidence of the natural vortex length and its effect on the separation efficiency of gas cyclones, Filtr. Sep. 32 (1995) 799–804.

[6] W. Peng, A.C. Hoffmann, H.W.A. Dries, M.A. Regelink, L.E. Stein, Experimental study of the vortex end in centrifugal separators: the nature of the vortex end, Chem. Eng. Sci. 60 (2005) 6919–6928.

[7] W. Peng, A.C. Hoffmann, H. Dries, Separation of swir tube separators, AIChE J. 53 (2007) 589–597.

[8] Fuping Qian, Mingyao Zhang, Study of the natural vortex length of a cyclone with response surface methodology, Comput. Chem. Eng. 29 (2005) 2155–2162.
[9] F. Qian, Y. Wu, Effects of the inlet section angle on the separation performance of a cyclone, Chem. Eng. Res. Des. 87 (2009) 1567–1572.
[10] F. Qian, X. Huang, M. Zhang, Study of gas shortcut flow rate in cyclone with different inlet section angles using response surface methodology, Int. J. Chem. React. Eng. 7 (2009) A30.
[11] A.C. Hoffmann, L.E. Stein, Gas Cyclones and Swirl Tubes, Principles, Design and Operation, second ed., Springer, Berlin, Heidelberg, New York, 2007.
[12] S. Bernado, M. Mori, A.P. Peres, R.P. Dionisio, 3-D computational fluid dynamics for gas and gas-particle flows in a cyclone with different inlet section angles, Powder Technol. 162 (2006) 190–200.
[13] G.I. Pisarev, V. Gjerde, B.V. Balakin, A.C. Hoffmann, H.A. Dijkstra, W. Peng, Experimental and computational study of the “end of the vortex” phenomenon in reverse-flow centrifugal separators, AIChE J. 58 (2012) 1371–1380.
[14] V. Gjerde, The natural vortex length in centrifugal separators, Master’s thesis, University of Groningen, Dept. of Physics and Technology, 2010.
[15] G. Gronald, J.J. Derksen, Simulating turbulent swirling flow in a gas cyclone: a comparison of various modeling approaches, Powder Technol. 205 (2011) 160–171.
[16] G.I. Pisarev, Experimental and numerical study of the End of the Vortex phenomenon, PhD thesis, University of Bergen, Dept. of Physics and Technology, 2011.
[17] A.I. Khuri, J.A. Cornell, Response Surfaces, Designs and Analyses, Marcel Dekker Inc., 1987.
[18] G.E.P. Box, N.R. Draper, Empirical Model-Building and Response Surfaces, Wiley & Sons Inc., 1987.
[19] R.H. Myers, D.C. Montgomery, Response Surface Methodology, Wiley, 1995.
[20] S. Chandrasekharan, R.C. Panda, B.N. Swaminathan, Statistical modeling of an integrated boiler for coal fired thermal power plant, Heliyon 4 (2018) e00322.
[21] A. Sonsiri, V. Punyakum, T. Radpukdee, Optimal variables estimation for energy reduction via a remote supervisory control: application to a counter-flow rotary dryer, Heliyon 5 (2019) E01087.
[22] J. Meyers, B.J. Geurts, P. Sagaut, Quality and Reliability of Large-Eddy Simulations, Springer, 2008.
[23] W. Griffiths, F. Boysan, Computational fluid dynamics (CFD) and empirical modelling of the performance of a number of cyclone samplers, J. Aerosol Sci. 27 (1996) 281–304.
[24] F. Boysan, W.H. Ayers, J.A. Swithenbank, A fundamental mathematical modeling approach to cyclone design, Trans. Inst. Chem. Eng. 60 (1982) 222–230.
[25] A.J. Hoekstra, J.J. Derksen, H.E.A. Van Den Akker, An experimental and numerical study of turbulent swirling flow in gas cyclones, Chem. Eng. Sci. 54 (1999) 2055–2065.
[26] A.J. Hoekstra, Gas Flow field and collection efficiency of cyclone separators, PhD thesis, Delft Technical University, 2000.
[27] J.J. Derksen, H.E.A. van den Akker, Simulation of the vortex core precession in a revrse flow cyclone, AIChE J. 46 (2002) 1317–1330.
[28] J.J. Derksen, Simulations of confined turbulent vortex flow, Comput. Fluids 34 (2005) 301–318.
[29] J.J. Derksen, S. Sundaresan, H.E.A. van den Akker, Simulation of mass-loading effects in gas-solid cyclone separators, Powder Technol. 163 (2006) 59–68.
[30] H.H. Rosenbrock, An automatic method for finding the greatest or least value of a function, Comput. J. 3 (1960) 175–184.